Robust Position Anti-Interference Control for PMSM Servo System With Uncertain Disturbance

Longfei Li, Jie Xiao, Yun Zhao, Kan Liu, Senior Member, *IEEE*, Xiaoyan Peng, Haozhe Luan, and Kaiqing Li

[1]***Abstract*—Aiming to suppress the influence of uncertain disturbances in the drive control of permanent magnet synchronous machines (PMSM), such as the parameter uncertainties and load disturbance, a robust anti-interference control for the angular position tracking control of a PMSM servo system has been proposed in this paper. During the position tracking, uncertain system disturbances being regarded as a lumped unknown term will be online observed by a nonlinear disturbance observer (NDOB), of which the influence will consequently be counteracted by a robust backstepping compensator (RBC). The asymptotical stability of proposed control scheme is analyzed and designed according to the Lyapunov stability criterion, and its convergence against the system uncertain disturbance is verified on a prototype PMSM servo platform and shows good performance in rotor angular position tracking and anti-interference.**

***Index Terms*—Nonlinear disturbance observer (NDOB), permanent magnet synchronous machine (PMSM), position control, robust backstepping compensator (RBC), servo system.**

I. INTRODUCTION

WITH the rapid development of power electronic devices, microcomputers and modern control theory, the permanent magnet synchronous machine (PMSM) have been widely used in the textile industry, industrial robots, medical equipment, household appliances, etc. [1], [2], thanks to its simple structure, light weight, high power density and strong driving capability. However, the performance of position and speed controls of PMSMs is usually sensitive to the machine nonlinearity, time-varying parameters, and external load disturbances, and a strong position locking ability is usually needed in applications such as robotic arms and marine steering gears[3]. In this case, the traditional linear control method is usually difficult to ensure the overall performance of servo system [4].

In order to overcome this issue, related nonlinear control methods such as the sliding mode variable structure control [5], [6], adaptive control [7], [8], model predictive control [9], [10], active disturbance rejection control (ADRC) [11], feedback linearization control [12] and adaptive backstepping control [20], [21] are widely investigated for solving the above problems. For example, A. T. Nguyen et al. [13] has proposed a model reference adaptive control (MRAC) based scheme, including an adaptive compensator and a feedback controller to improve the speed response against unknown external interference. However, the adaptive control scheme is usually difficult to eliminate the influence of unmodeled uncertainty. In this case, once the influence of uncertainty is out of a certain range, the resulting system chaotic responses will cause a deterioration of the system stability [14]. Besides, it is reported in some articles that the sliding mode control (SMC) is of high robustness and simple structure, which can guarantee the tracking accuracy in the presence of parameter uncertainty and external interference, and also can increase the control gain of the sliding mode surface to further improve the system robustness. However, a too large control gain tends to increase the chattering and then result in a deterioration of the control performance [15]-[17]. Similarly, Hebertt Sira-Ramírez et al. [18] employs an active disturbance rejection control (ADRC) scheme to overcome the influence of uncertain disturbance, which has a simple structure and can be easily operated in discrete time. However, it is difficult to properly adjust the parameter setups of the ADRC controller. Recently, a novel adaptive backstepping control (ARBC) is proposed in [19], which has taken into account the estimation of load torque for improving the rotor position tracking. Similarly, the ARBC with extended state observer (ESO) is also used to deal with the parameter uncertainty and external interference for the speed regulation of a wind turbine differential mechanism, while the unmodeled uncertainty of the system without consider [20]. Besides, the ARBC is also used to cooperate with the estimated moment of inertia and load torque to achieve good control performance under ultra-low speed control [21].

In this paper, a RBC combined with a nonlinear disturbance observer (NDOB) is proposed for the anti-interference position control of PMSM servo system, which has accounted for the influences of uncertain modeling errors and external disturbances. The proposed scheme has considered the influence of mismatched parameters of PMSM servo system and the overall system disturbances in current, torque, speed etc. Those disturbances are modeled as a lumped term and properly online compensated by the proposed method. Besides, the asymptotical stability of the proposed control scheme is analyzed and designed according to the Lyapunov stability criterion, which guarantees the stability and convergence of whole system. The performance of proposed method is finally verified on a prototype PMSM servo system, and shows quite good robustness against unknown parameters and external load

Manuscript was submitted for review on 25, October, 2019.

The work is supported by the financial support of National Natural Science Foundation of China under Grant 51877075 and 51575167, the State Key Laboratory of Advanced Design and Manufacturing for Vehicle Body (No. 71865008), Hunan University, and the State Key Laboratory of Reliability and Intelligence of Electrical Equipment (No. EERIKF2018007), Hebei University of Technology.

Longfei Li, Jie Xiao, Yun Zhao, Kan Liu, Xiaoyan Peng, Haozhe Luan and Kaiqing Li are with Hunan University.(e-mail: lfli@hnu.edu.cn)

Digital Object Identifier 10.30941/CESTEMS.2020.00020

disturbances.

II. PMSM MODEL

The mathematical model of PMSM on the *dq*-axis can be expressed as

$$\begin{cases} \dot{x}_1 = x_2 \\ \dot{x}_2 = \theta_1 x_3 - \theta_2 x_2 - \theta_3 \\ \dot{x}_3 = -g_1 x_3 - g_2 x_2 x_4 - g_3 x_4 + g_4 u_q + f_1 \\ \dot{x}_4 = -g_1 x_4 + g_2 x_2 x_3 + g_4 u_d + f_2 \end{cases} \tag{1}$$

where

$$\begin{aligned} &x_1 = \theta_m, x_2 = \omega_{\mathrm{m}}, x_3 = i_q, x_4 = i_d \\ &g_1 = \frac{R_{\mathrm{s}}}{L}, g_2 = P_{\mathrm{n}}, g_3 = \frac{P_{\mathrm{n}}\psi_f}{L}, g_4 = \frac{1}{L} \\ &\theta_1 = \frac{3P_n\psi_f}{2J}, \theta_2 = \frac{B}{J}, \theta_3 = \frac{T_L}{J} \end{aligned} \tag{2}$$

where i_d, i_q represent the *dq*-axis currents; u_d, u_q represent the *dq*-axis voltages; R_s, L, ψ_f and P_n represent the stator resistance, *dq*-axis inductances, permanent magnet flux linkage and the number of pole pairs, respectively; J, T_L and B represent the moment of inertia, the load torque and the viscous friction coefficient, respectively; θ_m, ω_m represent mechanical position angle and the rotor angular speed; f_1 and f_2 represent other uncertainties, including modeling errors, external disturbances, etc.

Taking into account the parameter variations, (1) can be expressed as

$$\begin{aligned} \dot{x}_2 &= \theta_1 x_3 - \theta_2 x_2 - \theta_3 \\ &= (\theta_{1n} + \Delta\theta_1)x_3 - (\theta_{2n} + \Delta\theta_2)x_2 - (\theta_{3n} + \Delta\theta_3) \\ &= \theta_{1n} x_3 - \theta_{2n} x_2 + d \end{aligned} \tag{3}$$

$$d = \Delta\theta_1 x_3 - \Delta\theta_2 x_2 - \theta_3 \tag{4}$$

where θ_{1n}, θ_{2n}, θ_{3n} are the nominal parameters; $\Delta\theta_1$, $\Delta\theta_2$, $\Delta\theta_3$ are the parameter variations, d represents the lumped disturbance, which includes internal parameter variations, external load disturbances, and other uncertainties.

To facilitate the controller design, the system needs to meet the following assumptions

Assumption 1: The lumped disturbance d is bounded and has a slow change with time

$$\begin{cases} |d| < \mu \\ \dot{d} \approx 0 \end{cases} \tag{5}$$

where μ represents the boundary value of d.

Assumption 2: Other uncertain terms f_1, f_2 satisfy the following conditions

$$\begin{cases} |f_1| \le h_1 \\ |f_2| \le h_2 \end{cases} \tag{6}$$

where h_1, h_2 represent the boundary values of f_1 and f_2, respectively

III. DESIGN OF POSITION CONTROL STRATEGY FOR PMSM

A. Design of Nonlinear Disturbance Observer

To reduce the influence of internal parameter variations and external load disturbances, a NDOB for compensation control is introduced.

To estimate the system disturbances, the NDOB [22] applied in this paper can be given as follows

$$\begin{cases} \hat{d} = p + lx_2 \\ \dot{p} = -lp - l\left[lx_2 - \theta_{2n}x_2 + \theta_{1n}x_3\right] \end{cases} \tag{7}$$

where $\hat{d}$, p, and l are estimates of the lumped system disturbance, intermediate variables of NDOB and gains of NDOB, respectively.

Define the disturbance error as e_d which satisfies the following conditions

$$\begin{cases} e_d = \hat{d} - d \\ |e_d| \le \xi \end{cases} \tag{8}$$

where ξ is the boundary value of the disturbance error e_d.

It can be proved that $\hat{d}$ will asymptotically approach the actual value d by selecting the appropriate parameter l.

Proof: By combined of (3), (7) and *Assumption 1*, $\dot{e}_d$ is got as follows

$$\begin{aligned} \dot{e}_d &= \dot{\hat{d}} - \dot{d} = \dot{p} + l\dot{x}_2 - \dot{d} \\ &= -lp - l\left[lx_2 - \theta_{2n}x_2 + \theta_{1n}x_3\right] + l[\theta_{1n}x_3 - \theta_{2n}x_2 + d] \\ &= -l(p + lx_2) + ld = -l(\hat{d} - d) = -le_d \end{aligned} \tag{9}$$

It is worth to note that $l > 0$ in (9) and magnitude of this parameter determines the speed of convergence, which means the convergence speed increases with l. The schematic diagram of NDOB is shown in Fig. 1. The advantage of the NDOB introduced in the paper is that its structure is much simpler and it can effectively estimate and compensate a wide range of uncertainty and interference without sacrificing the overall control performance.

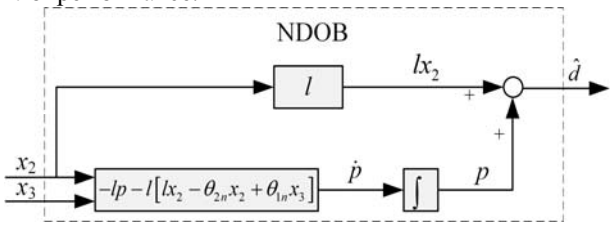

Fig. 1. Schematic diagram of NDOB

B. Design of Robust Backstepping Controller

The RBC can simplify the high-order system to several first-order subsystems by introducing virtual control variables [19], [20]. A RBC based on NDOB is proposed to control PMSM servo system considering parameter uncertainties and external load disturbances. The overall control block diagram of the RCB with NDOB is shown in Fig. 2.

According to the basic design principle of backstepping controller, the error variables z_1, z_2, z_3 and z_4 of the system can be defined as

$$\begin{cases} z_1 = x_1 - x_r \\ z_2 = x_2 - \alpha_1 \\ z_3 = x_3 - \alpha_2 \\ z_4 = x_4 \end{cases} \tag{10}$$

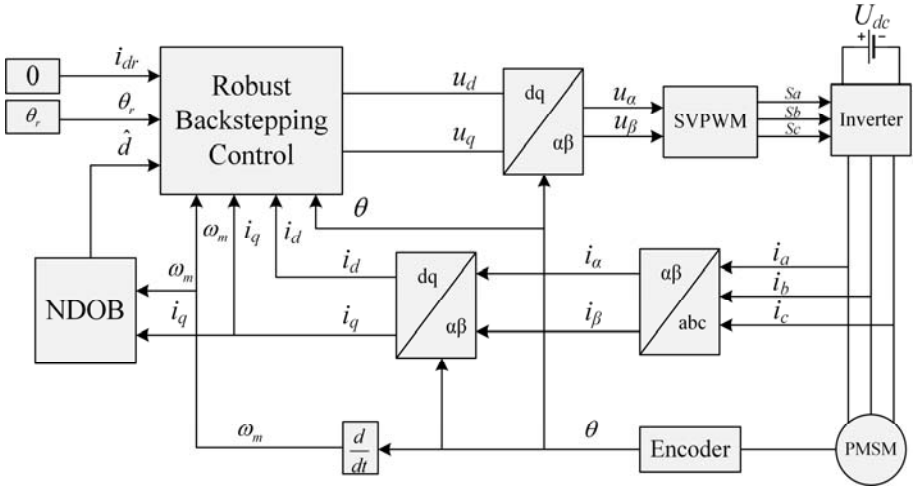

Fig. 2. Overall control block diagram of RBC with NDOB

where x_r is the desired signal; α_1, α_2 are the desired virtual control signals.

***Step 1*:** Select the first Lyapunov function V_1 as follows

$$V_1 = \frac{1}{2} z_1^2 \tag{11}$$

By differentiating (11), $\dot{V}_1$ can be obtain from (12)

$$\dot{V}_1 = z_1 \dot{z}_1 = z_1 (z_2 + \alpha_1 - \dot{x}_r) \tag{12}$$

The virtual control variable α_1 is represented as follows

$$\alpha_1 = -k_1 z_1 + \dot{x}_r \tag{13}$$

where k_1 is an adjustable positive parameter, $\dot{V}_1$ can be written as follows

$$\dot{V}_1 = -k_1 z_1^2 + z_1 z_2 \tag{14}$$

***Step 2*:** Select the second Lyapunov function V_2 as follows

$$V_2 = V_1 + \frac{1}{2} z_2^2 \tag{15}$$

By differentiating (15), $\dot{V}_2$ can be obtained below

$$\begin{aligned} \dot{V}_2 = \dot{V}_1 + z_2 \dot{z}_2 = -k_1 z_1^2 + \theta_{1n} z_2 z_3 + z_2 (z_1 + \\ \theta_{1n} \alpha_2 - \theta_{2n} x_2 + d + k_1 x_2 - k_1 \dot{x}_r - \ddot{x}_r) \end{aligned} \tag{16}$$

The virtual control variable α_2 is represented as follows

$$\begin{cases} \alpha_2 = \alpha_{2a} + \alpha_{2r} \\ \alpha_{2a} = -\dfrac{1}{\theta_{1n}} (z_1 - \theta_{2n} x_2 + \hat{d} + k_1 x_2 - k_1 \dot{x}_r - \ddot{x}_r + k_2 z_2) \end{cases} \tag{17}$$

where k_2 is an adjustable positive parameter, α_{2a} is the model compensation control to achieve tracking control and α_{2r} is the robust control rate used to reduce the effects of system uncertainties.

Combining (16) and (17) yields (18):

$$\begin{cases} \dot{V}_2 = \dot{V}_2 \mid_{equal} + \theta_{1n} z_2 z_3 \\ \dot{V}_2 \mid_{equal} = -k_1 z_1^2 - k_2 z_2^2 + z_2 (\theta_{1n} \alpha_{2r} - e_d) \end{cases} \tag{18}$$

According to (18), the selection of α_2 should meet the following conditions to ensure the system stability:

$$\begin{cases} z_2 \theta_{1n} \alpha_{2r} \le 0 \\ z_2 (\theta_{1n} \alpha_{2r} - e_d) \le \varepsilon_1 \end{cases} \tag{19}$$

where ε_1 is an arbitrarily small positive parameter which represents the attenuation level of system uncertainties.

Therefore, the robust control rate α_2 satisfies (19) can be chosen as

$$\alpha_{2r} = -\frac{\xi^2}{4 \theta_{1n} \varepsilon_1} z_2 \tag{20}$$

Proof: Combining (8), (19) and (20) yields (21):

$$\begin{aligned} z_2 (\theta_{1n} \alpha_{2r} - e_d) &\le -\frac{\xi^2}{4\varepsilon_1} z_2^2 + \xi |z_2| \\ &= -\left(\frac{\xi |z_2|}{2\sqrt{\varepsilon_1}} - \sqrt{\varepsilon_1} \right)^2 + \varepsilon_1 \le \varepsilon_1 \end{aligned} \tag{21}$$

***Step 3*:** Select the third Lyapunov function V_3 as follows

$$V_3 = V_2 + \frac{1}{2} z_3^2 \tag{22}$$

By differentiating z_3, $\dot{z}_3$ can be obtained below

$$\begin{aligned} \dot{z}_3 &= \dot{x}_3 - \dot{\alpha}_2 = \dot{x}_3 - \varphi_1 + \varphi_2 \dot{x}_2 \\ &= -g_1 x_3 - g_2 x_2 x_4 - g_3 x_4 + g_4 u_q + f - \varphi_1 + \varphi_2 \dot{x}_2 \end{aligned} \tag{23}$$

where

$$\begin{cases} \varphi_1 = \dfrac{1}{\theta_{1n}} [(k_1 + k_2) \ddot{x}_r + \dddot{x}_r - \ddot{\hat{d}} - (1 + k_1 k_2)(x_2 - \dot{x}_r) + \dfrac{\xi^2}{4\varepsilon_1} z_2] \\ \varphi_2 = \dfrac{1}{\theta_{1n}} (\dfrac{\xi^2}{4\varepsilon_1} + k_1 + k_2 - \theta_{2n}) \end{cases} \tag{24}$$

By combining (22) and (23), $\dot{V}_3$ is derived as follows

$$\begin{aligned} \dot{V}_3 = \dot{V}_2 \mid_{equal} - g_2 x_2 z_3 z_4 + z_3 (\theta_{1n} z_2 - g_1 x_3 - g_3 x_2 \\ + g_4 u_q + f_1 - \varphi_1 + \varphi_2 \theta_{1n} x_3 - \varphi_2 \theta_{2n} x_2 + \varphi_2 \hat{d} - \varphi_2 e_d) \end{aligned} \tag{25}$$

According to (25), the expression of control output u_q is expressed as follows

$$\begin{cases} u_q = u_{qa} + u_{qr} \\ u_{qa} = -\dfrac{1}{g_4} \begin{pmatrix} \theta_{1n} z_2 - g_1 x_3 - g_3 x_2 - \varphi_1 + \\ \varphi_2 \theta_{1n} x_3 - \varphi_2 \theta_{2n} x_2 + \varphi_2 \hat{d} + k_3 z_3 \end{pmatrix} \end{cases} \tag{26}$$

where k_3 is an adjustable positive parameter, u_{qa} is the model

compensation control, u_{qr} is the robust control rate.

By combining (25) and (26), (27) can be obtained as follows

$$\begin{cases} \dot{V}_3 = \dot{V}_3 \mid_{equal} -g_2 x_2 z_3 z_4 \\ \dot{V}_3 \mid_{equal} = \dot{V}_2 \mid_{equal} -k_3 z_3^2 + z_3(g_4 u_{qr} + f_1 - \varphi_2 e_d) \end{cases} \tag{27}$$

Similarly, the selection of u_{qr} should meet the following conditions

$$\begin{cases} z_3 g_4 u_{qr} \le 0 \\ z_3(g_4 u_{qr} + f_1 - \varphi_2 e_d) \le \varepsilon_2 + \varepsilon_{2r} \end{cases} \tag{28}$$

where ε_2, ε_{2r} are arbitrarily small positive parameters.

Therefore, the robust control rate u_{qr} can be chosen as follows

$$u_{qr} = -\frac{z_3}{g_4}\left(\frac{h_1^2}{4\varepsilon_2} + \frac{(\varphi_2 \xi)^2}{4\varepsilon_{2r}}\right) \tag{29}$$

Proof: By combining (6), (8), (28) and (29), (30) can be derived as follows

$$\begin{aligned} & z_3(g_4 u_{qr} + f_1 - \varphi_2 e_d) \\ & \le -\left(\frac{h_1^2}{4\varepsilon_2} + \frac{(\varphi_2 \xi)^2}{4\varepsilon_{2r}}\right) z_3^2 + h_1 |z_3| + \xi |\varphi_2| |z_3| \\ & = -\left(\frac{h_1 |z_3|}{2\sqrt{\varepsilon_2}} - \sqrt{\varepsilon_2}\right)^2 - \left(\frac{|\varphi_2| \xi |z_3|}{2\sqrt{\varepsilon_{2r}}} - \sqrt{\varepsilon_{2r}}\right)^2 + \varepsilon_2 + \varepsilon_{2r} \\ & \le \varepsilon_2 + \varepsilon_{2r} \end{aligned} \tag{30}$$

***Step 4*:** Select the last Lyapunov function V_4 as follows

$$V_4 = V_3 + \frac{1}{2} z_4^2 \tag{31}$$

By differentiating (30), $\dot{V}_4$ can be obtained as follows

$$\dot{V}_4 = \dot{V}_3 \mid_{equal} + z_4(-g_2 x_2 z_3 - g_1 x_4 + g_2 x_2 x_3 + g_4 u_d + f_2) \tag{32}$$

Similarly, according to (31), the control output u_d is expressed as follows

$$\begin{cases} u_d = u_{da} + u_{dr} \\ u_{da} = -\frac{1}{g_4}(-g_2 x_2 z_3 - g_1 x_4 + g_2 x_2 x_3 + k_4 z_4) \end{cases} \tag{33}$$

where k_4 is an adjustable positive parameter, u_{da} is the model compensation control to achieve tracking control, u_{dr} is the robust control rate.

By combining (32) and (33), (34) is got as follows

$$\dot{V}_4 = \dot{V}_3 \mid_{equal} -k_4 z_4^2 + z_4(g_4 u_{dr} + f_2) \tag{34}$$

Similarly, u_{dr} should meet the following conditions:

$$\begin{cases} z_4 g_4 u_{dr} \le 0 \\ z_4(g_4 u_{dr} + f_2) \le \varepsilon_3 \end{cases} \tag{35}$$

where ε_3 is an arbitrarily small positive parameter.

Therefore, the robust control rate u_{dr} can be chosen as follows

$$u_{dr} = -\frac{h_2^2}{4 g_4 \varepsilon_3} z_4 \tag{36}$$

Proof: Combined (6), (35) and (36), (37) can be derived as follows

$$\begin{aligned} z_4(g_4 u_{dr} + f_2) & \le -\frac{h_2^2}{4\varepsilon_3} z_4^2 + h_2 |z_2| \\ & = -\left(\frac{h_2 |z_4|}{2\sqrt{\varepsilon_3}} - \sqrt{\varepsilon_3}\right)^2 + \varepsilon_3 \le \varepsilon_3 \end{aligned} \tag{37}$$

C. Stability Analysis

Construct a Lyapunov function V as follows

$$V(t) = V_4 = \frac{1}{2} z_1^2 + \frac{1}{2} z_2^2 + \frac{1}{2} z_3^2 + \frac{1}{2} z_4^2 \tag{38}$$

By combining (19), (28), (35) and (34), $\dot{V}$ can be obtained below

$$\begin{aligned} \dot{V}(t) & = -k_1 z_1^2 - k_2 z_2^2 - k_3 z_3^2 - k_4 z_4^2 + z_2(\theta_{1n} \alpha_{2r} - e_d) \\ & \quad + z_3(g_4 u_{qr} + f_1 - \varphi_2 e_d) + z_4(g_4 u_{dr} + f_2) \\ & \le -k_1 z_1^2 - k_2 z_2^2 - k_3 z_3^2 - k_4 z_4^2 + \varepsilon_1 + \varepsilon_2 + \varepsilon_{2r} + \varepsilon_3 \\ & \le -2kV(t) + \varepsilon \end{aligned} \tag{39}$$

where

$$\begin{cases} k = \min(k_1, k_2, k_3, k_4) \\ \varepsilon = \varepsilon_1 + \varepsilon_2 + \varepsilon_{2r} + \varepsilon_3 \end{cases} \tag{40}$$

The solution of differential equation of (39) can be expressed as follows

$$V(t) \le e^{-2kt} V(0) + \frac{\varepsilon}{2k}(1 - e^{-2kt}) \tag{41}$$

According to (41), it can be determined that the closed-loop control system is asymptotically stable, and its exponential convergence rate is k, and the final convergence error e satisfies following formula

$$|e| \le \lim_{t \to \infty} V(t) = \frac{\varepsilon}{2k} \tag{42}$$

Therefore, the convergence speed and error of the control system can be changed by adjusting the parameters ε and k.

IV. Experimental verification

In this section, a Speed_goat control platform is adopted to drive a 750W surface mounted PMSM to verify the effectiveness of the proposed control strategy. In order to test the performance under different conditions, the external load will be given by the magnetic powder brake, heavy hammer and DC load motor, respectively. The experimental platform and parameters of PMSM are shown in Fig. 4 and TABLE I, respectively. The DC bus voltage is 60V and the IGBT switching frequency is 10kHz. The speed measurement uses the M/T hybrid measurement method integrated in Speed_goat control platform. In addition, a 2500-lines incremental encoder has been applied to achieve an accurate measurement of speed, which cooperates with a low-pass filter for the sake of suppressing high frequency noise. The performance of the proposed control in this paper is compared with the optimal PI control with and without NDOB. The latter two control methods are briefly introduced in the Appendix. The related parameters of the three control methods are given below

(1) RBC with NDOB: the control gain of the NDOB is selected as l = 200; the boundary value h_1, h_2 of the uncertain

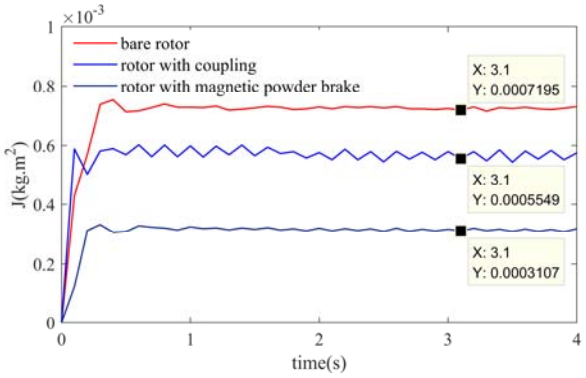

(a)

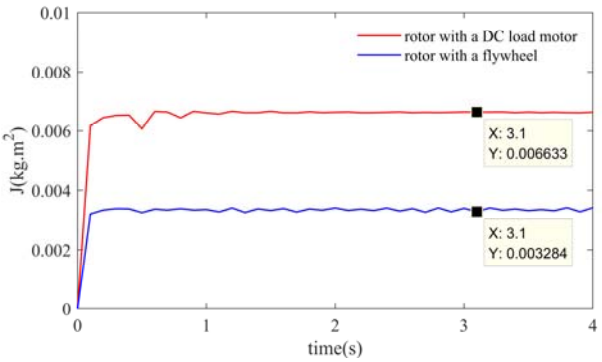

(b)

Fig. 3. Estimated combined moment of inertia of PMSM under different conditions. (a) bare rotor, rotor with coupling and with magnetic powder brake, respectively. (b) rotor with a flywheel and with a DC load motor, respectively

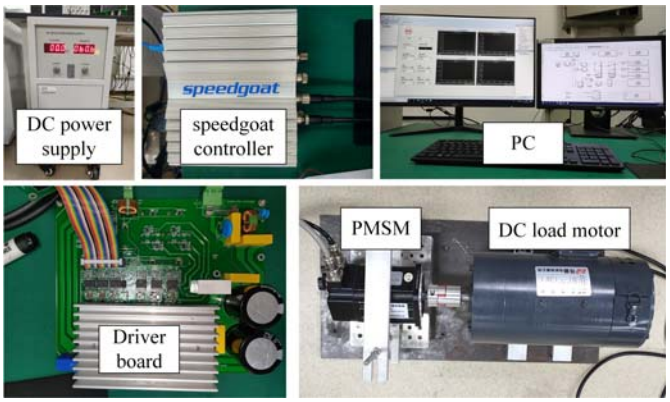

Fig. 4. Speedgoat controller based PMSM test rig.

TABLE I
PARAMETERS OF PMSM

Symbol	PMSM parameters	Value
U_N	rated voltage	220V
I_N	rated current	3A
P_N	rated power	750W
T_N	rated torque	2.4N·m
n_N	rated speed	3000r/min
R_s	stator resistance	1.86Ω
L	dq-axis inductances	2.8mH
ψ_f	permanent magnet flux linkage	0.109Wb
P_n	number of pole pairs	4
J	moment of inertia of bare rotor	2.95×10^{-4}kg·m^2
B	viscous friction coefficient	0.001

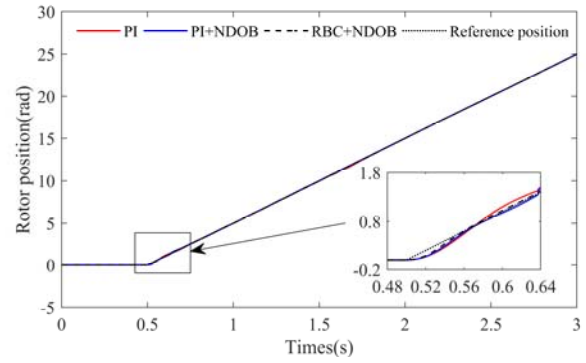

(a)

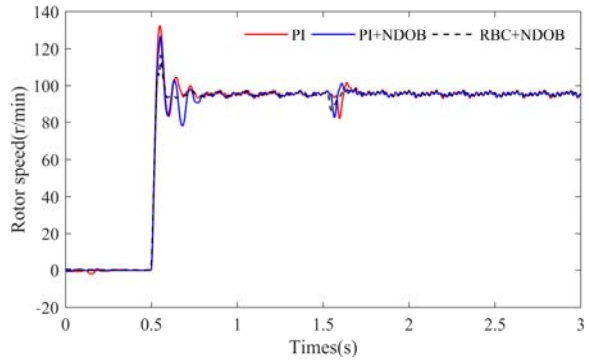

(b)

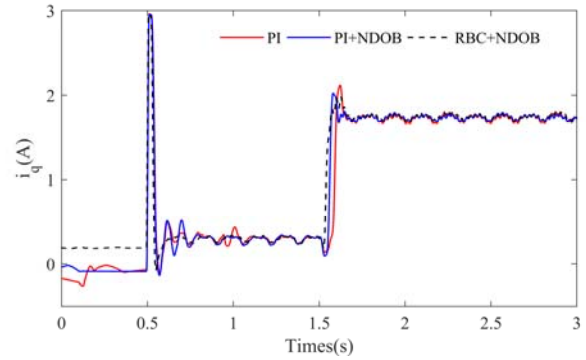

(c)

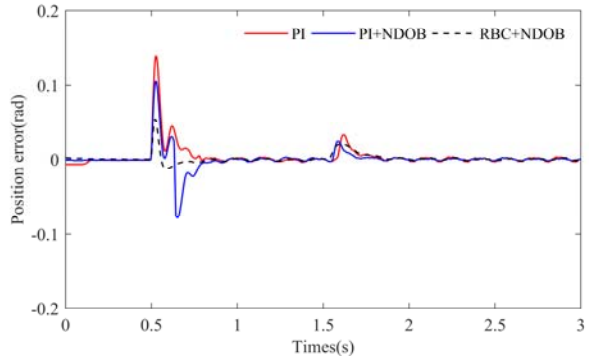

(d)

Fig. 5. Comparative experimental tests with an addition of external load T_L=1N·m at t=1.5s. (a) rotor position. (b) rotor speed. (c) q-axis current. (d) rotor position error

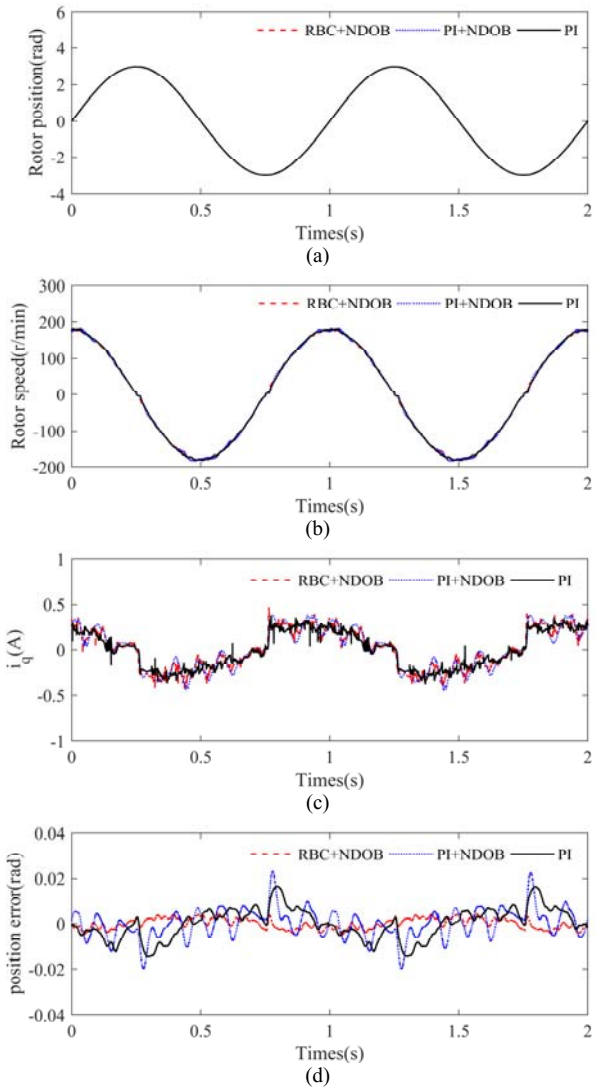

Fig. 6. Sinusoidal position tracking test at no load condition. (a) rotor position. (b) rotor speed. (c) q-axis current. (d) rotor position error.

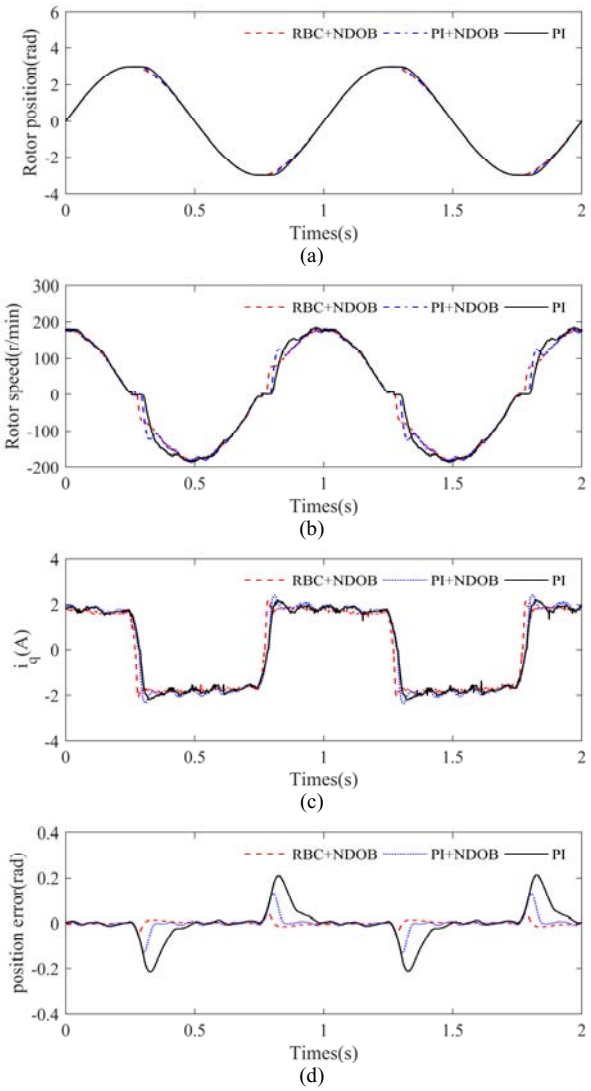

Fig. 7. Sinusoidal position tracking in loaded condition. (a) rotor position. (b) rotor speed. (c) q-axis current. (d) rotor position error.

variable f_1, f_2 is set as $h_1 = h_2$=20; the boundary value ξ of the disturbance error is set to ξ = 10; RBC control parameters are set as k_1 = 50, k_2 = 100, k_3 = 500, k_4 = 200, ε_1 = 100, ε_2 = 200, ε_{2r} = 0.01, ε_3 = 0.01.

(2) Optimal PI: according to the optimal PI control method introduced in the Appendix, the control parameters are set to ω_i = 2π×600rad/s, ω_s = 2π×30rad/s, ω_p = 2π×6 rad/s.

(3) Optimal PI with NDOB: this control method is introduced in the Appendix, and its PI control constants and NDOB gain are the same as hereinbefore.

To optimize the performance of PI control, a moment of inertia identification experiment of PMSM is carried out. The identification method is also introduced in the Appendix, and the experimental results are shown in Fig. 3. The moment of inertia of bare rotor, rotor with coupling, rotor with magnetic powder brake, rotor with flywheel and rotor with DC load motor are 3.11×10^{-4}kg·m^2, 5.55×10^{-4}kg·m^2, 7.2×10^{-4}kg·m^2, 3.28×10^{-3}kg·m^2 and 6.63×10^{-3}kg·m^2, respectively.

(1) Tracking the slope change of rotor position: In the comparative experiment, the PMSM is loaded by a DC load motor. As shown in Fig. 5, the reference rotor position of PMSM is $\theta_r = 10\cdot(t\text{-}0.5)$ rad at t = 0.5s and the motor is loaded with 1N·m at t = 1.5s. As can be seen from Fig. 5(a) that the proposed method has less fluctuation during the position tracking. It can be seen that the proposed method has high tracking accuracy and can quickly converge to a given position even if there is an abrupt change in the external load as shown in Fig. 5(d). Fig. 8 (a) is the observed torque of NDOB, which settles down to 0 N·m between 0 and 0.5s. Further, it fluctuates around 0.05 N·m from 0.5s to 1.5s, then after 1.5s, it fluctuates around 1.05 N·m. It is obvious that the observed result of the NDON algorithm can quickly converge to the true value within 0.06s even there is a load change.

(2) Tacking the sinusoidal change of rotor position: As shown in Figs. 6 and 7, the comparative experiments with and without external load torque (1N·m), have the same sinusoidal input θ_r=3·sin(2π·t) rad. It can be seen that the proposed method has smoother speed and current responses compared to the other two control schemes. Fig. 6(d) and Fig. 7(d) show that at no load condition, the dynamic position errors $|e_\theta|$ ($e_\theta = \theta_r$-θ_m)

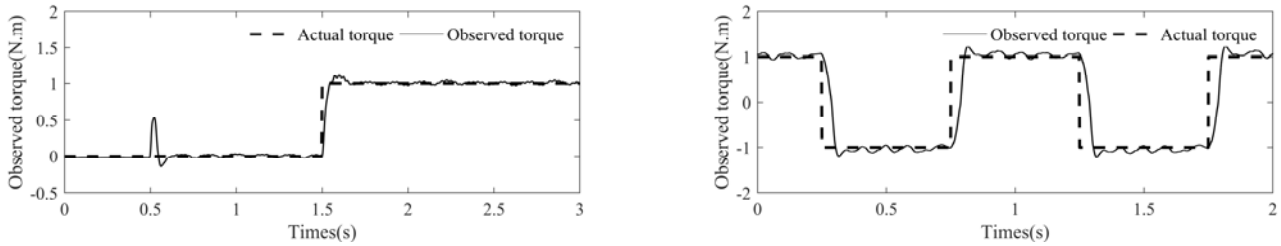

Fig. 8. Observed torque of NDOB. (a) suddenly add a load of 1N·m at t = 1.5s. (b) square wave load with 1N·m

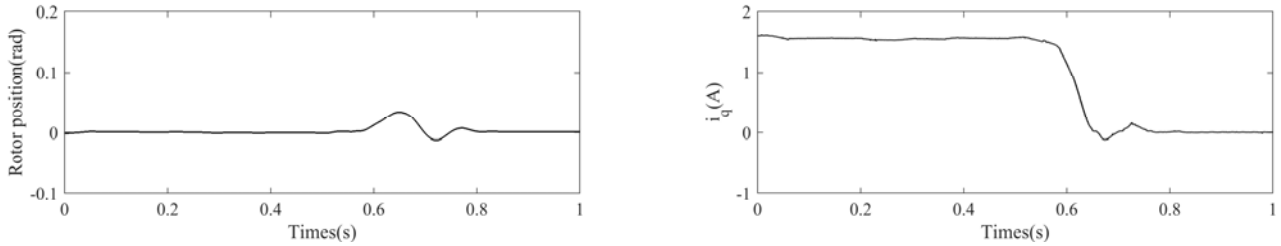

Fig. 9. Curve of PMSM rotor lock performance (RBC with NDOB). (a) rotor position. (b) *q*-axis current

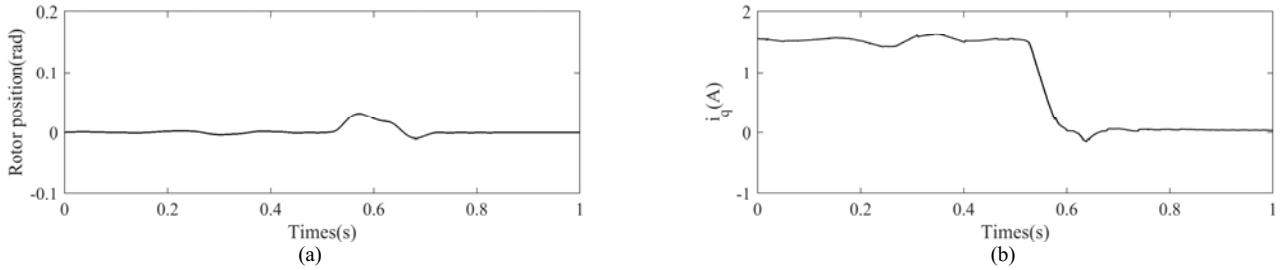

Fig. 10. Curve of PMSM rotor lock performance (PI control with NDOB). (a) rotor position. (b) *q*-axis current

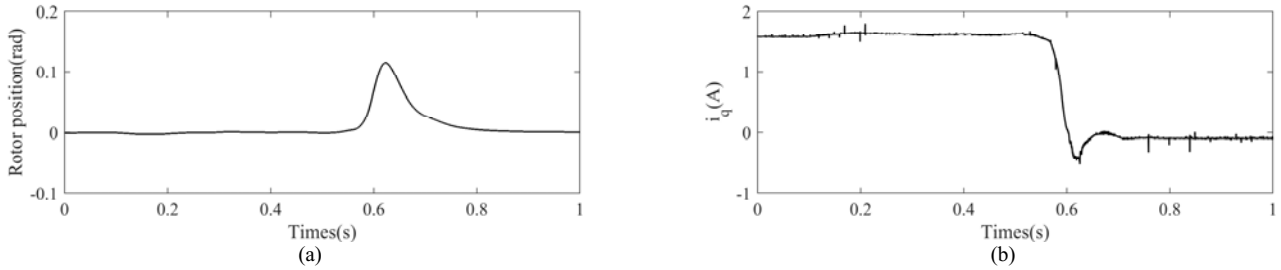

Fig. 11. Curve of PMSM rotor lock performance (PI control). (a) rotor position. (b) *q*-axis current

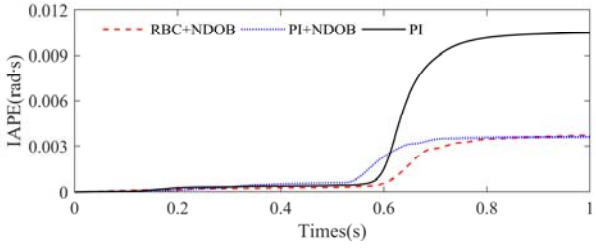

Fig. 12. Curve of integral absolute position error (IAPE = $\int_0^t |e_\theta(\tau)| d\tau$)

of three control methods (PI, PI+NDOB and RBC+NDOB) are less than 0.02rad, 0.025rad and 0.01rad, respectively, while in loaded condition T_L = 1N·m, $|e_\theta|$ is less than 0.2rad, 0.15rad and 0.05rad, respectively. Therefore, the proposed method has less position tracking errors at both no load and loaded conditions. Fig. 8(b) is the corresponding observed torque result of NDOB under load (1 N·m). It can be seen from the results of Fig. 8 that the proposed NDOB shows faster convergence speed and accuracy. According to the comparison tests shown in Figs. 5-7, it can be seen that the proposed method is robust to the variation of the load's moment of inertia.

(3) Holding the rotor position: In this experiment, the PMSM rotor will be held to the position of zero rad and connected to a flywheel with a heavy hammer and the weight will be removed at t = 0.5s. The equivalent load of the PMSM after the addition of a heavy hammer is about T_L = 0.88N·m. From the results shown in Fig. 9-11, it can be seen that the RBC+NDOB and PI+NDOB control have a small position change once the heavy hammer is removed. Furthermore, as can be seen in Fig. 12, which is the curve of integrated absolute position error (IAPE), it shows that the RBC+NDOB and PI+NDOB control have better anti-interference (when t=1s, IAPE of RBC+NDOB is 3.56×10^{-4}rad·s, IAPE of PI+NDOB is 3.66×10^{-4}rad·s and IAPE of PI is 10.46×10^{-4}rad·s). Besides, since the estimation error of the NDOB may cause an over-compensation or under-compensation in *q*-axis current, the employed RBC will eliminate this kind of influence to achieve a better control performance.

According to above experiments, it is proved that the proposed method has a high position tracking accuracy and a good anti-interference performance.

V. Conclusion

In this paper, a RBC with NDOB is proposed with considering the influence of uncertain system disturbances such as the parameter uncertainties and load disturbance. The proposed method estimates the lumped unknown terms by the NDOB and can effectively improves the robustness of the system through the application of RBC. Its tracking performance and robustness are analyzed and design according to the Lyapunov theorem, which ensures that the proposed control method is asymptotically stable. Further comparative experiment tests on a prototype PMSM servo system indicate that the proposed method has a high position tracking performance and good robustness against unknown parameters and external load disturbances. A further consideration on the resonance suppression and anti-interference control of two mass servo systems will be reported in future works.

Appendix

A. Optimal PI Control

According to the methods described in [23] and [24], the expression of the optimal PI control as follows, and its control block diagram is shown in Fig. 13.

1) PI control expression for current regulator

$$\begin{cases} u_d = (k_{pd} + \dfrac{k_{id}}{s})(i_d^* - i_d) \\ u_q = (k_{pq} + \dfrac{k_{iq}}{s})(i_q^* - i_q) \end{cases} \tag{43}$$

where k_{pd}, k_{pq} are the proportional gains; k_{id}, k_{iq} are the integral gains.

In this paper, $L_d = L_q = L$, so the PI parameter of the current regulator is given by the following expression

$$\begin{cases} k_{pd} = k_{pq} = \omega_i \cdot L \\ k_{id} = k_{iq} = \omega_i \cdot R_s \end{cases} \tag{44}$$

where ω_i is desired bandwidth of current regulator.

2) PI control expression for speed regulator

$$i_q^* = (k_{ps} + \frac{k_{is}}{s})(\omega_m^* - \omega_m) \tag{45}$$

where k_{ps} and k_{is} are the proportional gains and the integral gains, their values are given by the following expression

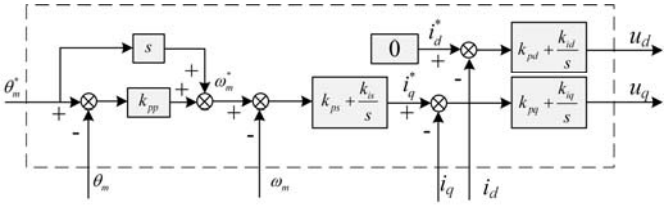

Fig. 13. Block diagram of the optimal PI

$$\begin{cases} k_{ps} = \omega_s \cdot J \\ k_{is} = \omega_s \cdot B \end{cases} \tag{46}$$

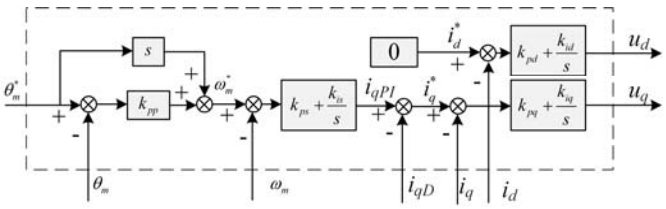

Fig. 14. Block diagram of the optimal PI with NDOB

where ω_s is desired bandwidth of speed regulator.

3) PI control expression for position regulator

$$\omega_m^* = k_{pp}(\theta_m^* - \theta_m) + s\theta_m^* \tag{47}$$

where k_{pp} is the proportional gain which is as follows

$$k_{pp} = \omega_p \tag{48}$$

where ω_p is desired bandwidth of position regulator.

It is obvious from (44)-(48) that PI constants of each regulator are related to PMSM parameters such as *dq*-axis inductances, the stator resistance, the moment of inertia of rotor and the friction coefficient. In servo control system, different control objects correspond to different moments of inertia and identifying the moment of inertia before designing the speed loop control is needed. Therefore, this paper mainly considers the influence of the moment of inertia to the optimized PI.

A moment of inertia identification is proposed to optimize speed regulator in [23]. The core of this method is to give a sinusoidal current on the *q*-axis to produce a sinusoidal speed at steady state, and the moment of inertia can be calculated by finding the zero crossing of the speed. The expression of this method is as follows

$$J = \frac{1.5 P_n \psi_f i_{qp} \sin(\omega_h t_0)}{\omega_p \omega_h} \tag{49}$$

where i_{qp}, ω_h are the magnitude and angular frequency of the given *q*-axis sinusoidal current; t_0 represents the time point when the speed is zero; ω_p is the magnitude of sinusoidal angular speed at steady state.

B. Optimal PI Control with NDOB

According to (3), the expression of i_q is shown as follows and its control block diagram is shown in Fig. 14

$$i_q = \frac{\theta_{2n}\omega_m + \dot{\omega}_m}{\theta_{1n}} - \frac{d}{\theta_{1n}} \tag{50}$$

$$i_q^* = i_{qPI} - i_{qD} = (k_{ps} + \frac{k_{is}}{s})(\omega_m^* - \omega_m) - \frac{\hat{d}}{\theta_{1n}} \tag{51}$$

where i_{qPI}, i_{qD} are the speed PI control output and compensation current.

References

[1] S. Fang, H. Liu, H. Wang, H. Yang and H. Lin, "High power density PMSM with lightweight structure and high-performance soft magnetic alloy core," *IEEE Transactions on Applied Superconductivity*, vol. 29, no. 2, pp. 1-5, Mar. 2019.

[2] R. Zhu, "Vertical GaN power transistor with intrinsic reverse conduction and low gate charge for high-performance power conversion," *IEEE Journal of Emerging and Selected Topics in Power Electronics*, vol. 7, no. 3, pp. 1449-1455, Sept. 2019.

[3] J. Lara, J. Xu and A. Chandra, "Effects of rotor position error in the

performance of field-oriented-controlled PMSM drives for electric vehicle traction applications," *IEEE Transactions on Industrial Electronics*, vol. 63, no. 8, pp. 4738-4751, Aug. 2016.

[4] R. Errouissi, A. Al-Durra and S. M. Muyeen, "Experimental validation of a novel PI speed controller for AC motor drives with improved transient performances," *IEEE Transactions on Control Systems Technology*, vol. 26, no. 4, pp. 1414-1421, Jul. 2018.

[5] X. Liu, H. Yu, J. Yu and L. Zhao, "Combined speed and current terminal sliding mode control with nonlinear disturbance observer for PMSM drive," *IEEE Access*, vol. 6, pp. 29594-29601, 2018.

[6] Z. Yin, L. Gong, C. Du, J. Liu and Y. Zhong, "Integrated position and speed loops under sliding-mode control optimized by differential evolution algorithm for PMSM drives," *IEEE Transactions on Power Electronics*, vol. 34, no. 9, pp. 8994-9005, Sept. 2019.

[7] G. Li, W. Xu, J. Zhao, S. Wang and B. L. (2017, Aug.), "Precise robust adaptive dynamic surface control of permanent magnet synchronous motor based on extended state observer," *IET Science, Measurement & Technology*, vol. 11, no. 5, pp. 590-599, Aug. 2017.

[8] H. H. Choi, N. T. Vu and J. Jung, "Digital implementation of an adaptive speed regulator for a PMSM," *IEEE Transactions on Power Electronics*, vol. 26, no. 1, pp. 3-8, Jan. 2011.

[9] R. Errouissi, A. Al-Durra, S. M. Muyeen and S. Leng, "Continuous-time model predictive control of a permanent magnet synchronous motor drive with disturbance decoupling," *IET Electric Power Applications*, vol. 11, no. 5, pp. 697-706, May. 2017.

[10] L. Samaranayake and S. Longo, "Degradation control for electric vehicle machines using nonlinear model predictive control," *IEEE Transactions on Control Systems Technology*, vol. 26, no. 1, pp. 89-101, Jan. 2018.

[11] C. Dai, J. Yang, Z. Wang and S. Li, "Universal active disturbance rejection control for non-linear systems with multiple disturbances via a high-order sliding mode observer," *IET Control Theory & Applications*, vol. 11, no. 8, pp. 1194-1204, May. 2017.

[12] H. Angue Mintsa, R. Venugopal, J. Kenne and C. Belleau, "Feedback linearization-based position control of an electrohydraulic servo system with supply pressure uncertainty," *IEEE Transactions on Control Systems Technology*, vol. 20, no. 4, pp. 1092-1099, Jul. 2012.

[13] A. T. Nguyen, M. S. Rafaq, H. H. Choi and J. Jung, "A model reference adaptive control based speed controller for a surface-mounted permanent magnet synchronous motor drive," *IEEE Transactions on Industrial Electronics*, vol. 65, no. 12, pp. 9399-9409, Dec. 2018.

[14] J. Yao, Z. Jiao, D. Ma and L. Yan, "High-accuracy tracking control of hydraulic rotary actuators with modeling uncertainties," *IEEE/ASME Transactions on Mechatronics*, vol. 19, no. 2, pp. 633-641, Apr. 2014.

[15] K. Zhao et al, "Robust model-free nonsingular terminal sliding mode control for PMSM demagnetization fault," *IEEE Access*, vol. 7, pp. 15737-15748, 2019.

[16] X. Zhang, L. Sun, K. Zhao and L. Sun, "Nonlinear speed control for PMSM system using sliding-mode control and disturbance compensation techniques," *IEEE Transactions on Power Electronics*, vol. 28, no. 3, pp. 1358-1365, Mar. 2013.

[17] J. Yang, S. Li and X. Yu, "Sliding-mode control for systems with mismatched uncertainties via a disturbance observer," *IEEE Transactions on Industrial Electronics*, vol. 60, no. 1, pp. 160-169, Jan. 2013.

[18] H. Sira-Ramírez, J. Linares-Flores, C. García-Rodríguez and M. A. Contreras-Ordaz, "On the control of the permanent magnet synchronous motor: an active disturbance rejection control approach," *IEEE Transactions on Control Systems Technology*, vol. 22, no. 5, pp. 2056-2063, Sept. 2014.

[19] X. Sun, H. Yu, J. Yu and X. Liu, "Design and implementation of a novel adaptive backstepping control scheme for a PMSM with unknown load torque," *IET Electric Power Applications*, vol. 13, no. 4, pp. 445-455, Apr. 2019.

[20] W. Yin, X. Wu and X. Ru, "Adaptive robust backstepping control of the speed regulating differential mechanism for wind turbines," *IEEE Transactions on Sustainable Energy*, vol. 10, no. 3, pp. 1311-1318, Jul. 2019.

[21] Y. Yu, Z. Mi, X. Guo, Y. Xu and T. Zhao, "Low speed control and implementation of permanent magnet synchronous motor for mechanical elastic energy storage device with simultaneous variations of inertia and torque," *IET Electric Power Applications*, vol. 10, no. 3, pp. 172-180, Mar. 2016.

[22] J. Yang, W. -. Chen and S. Li, "Non-linear disturbance observer-based robust control for systems with mismatched disturbances/uncertainties," *IET Control Theory & Applications*, vol. 5, no. 18, pp. 2053-2062, Dec. 2011.

[23] K. Liu and Z. Zhu, "Fast Determination of Moment of inertia of permanent magnet synchronous machine drives for design of speed loop regulator," *IEEE Transactions on Control Systems Technology*, vol. 25, no. 5, pp. 1816-1824, Sept. 2017.

[24] S. Yang and K. Lin, "Automatic control loop tuning for permanent-magnet AC servo motor drives," *IEEE Transactions on Industrial Electronics*, vol. 63, no. 3, pp. 1499-1506, Mar. 2016.

Longfei Li was born in Hunan, China, in 1996. He received the engineering degree in College of Engineering, Hunan Agricultural University, Changsha, China, 2014. He is currently working toward the M.S. degree in College of Mechanical and Vehicle Engineering, Hunan University, Changsha, China. His main research interests are design of driving algorithm for precision permanent magnet synchronous servo motor and the smallest servo hardware control board based on the wide-bandgap SiC power devices.

Jie Xiao was born in Hunan, China, in 1996. He received engineering degree, College of Machine, Jiangsu University, Zhenjiang, China, 2014. He is currently working toward the M.S. degree in College of Mechanical and Vehicle Engineering, Hunan University, Changsha, China. His current research interests include Servo control of permanent magnet synchronous motor and wide-bandgap switch device.

Zhao Yun was born in the Inner Mongolia Autonomous Region, China, in 1995. She received engineering degree, College of Transportation, Northeast Forestry University, Harbin, China, 2014 and currently is studying in College of Mechanical and Vehicle Engineering, Hunan University, Changsha, China. Her research interests include permanent magnet synchronous motor drives, maximum torque per ampere control.

Kan Liu (M'14-SM'17) received the B.Eng. and Ph.D. degrees in Automation from the Hunan University, China, in 2005 and 2011, respectively, and the Ph.D. degree in Electronic and Electrical Engineering from the University of Sheffield, Sheffield, U.K., in 2013. From 2013 to 2016, he was a research associate with the Department of Electronic and Electrical Engineering, the University of

Sheffield. From 2016 to 2017, he was a lecturer with the Control Systems Group of the Loughborough University. He is currently a Professor of Electro-mechanical Engineering at the Hunan University. His research interests include parameters estimation and sensorless control of permanent magnet synchronous machine drives and compensation of inverter nonlinearity, for applications ranging from electric vehicles, locomotives to servo systems. Prof. Liu serves as an Associate Editor for the IEEE Access, and the CES Transactions on Electrical Machines and Systems. He is also the Executive Director of the Engineering Research Center of the Ministry of Education on Automotive Electronics and Control Technology.

Xiaoyan Peng received the B.S. and M.S. degrees in mechanical engineering, and the Ph.D. degree in automatic control from Hunan University, Changsha, China, in 1986, 1989, and 2013, respectively. She is currently a Professor with the College of Mechanical and Vehicle Engineering, Hunan University, Changsha, China. Her research interests include control of mechatronic systems and safety analysis of autonomous vehicles.

Haozhe Luan was born in Shandong, China, in 1995. He received B.S. degree from Harbin University of Science and Technology, Harbin, China, 2014. He is currently working toward the Ph.D. degree in College of Mechanical and Vehicle Engineering, Hunan University, Changsha, China. His main research interests include DC/DC converters, and power factor correction.

Kaiqing Li received the B.S degree in electrical engineering and automation from Hunan Institute of Engineering, Xiangtan, China, in 2017. He is currently working toward the M.S. degree in control engineering in the College of Electrical and Information Engineering, Hunan University. His current research interests include parameters estimation and permanent magnet synchronous motor drive.